JOC The Journal of Organic Chemistry

Article

pubs.acs.org/joc

P(═O)H to P−OH Tautomerism: A Theoretical and Experimental Study

Benjamin G. Janesko,* Henry C. Fisher, Mark J. Bridle, and Jean-Luc Montchamp*

Department of Chemistry, Texas Christian University, Box 298860, Fort Worth, Texas 76129, United States

Supporting Information

ABSTRACT: Phosphinylidene compounds $R^1R^2P(O)H$ are important functionalities in organophosphorus chemistry and display prototropic tautomerism. Quantifying the tautomerization rate is paramount to understanding these compounds' tautomerization behavior, which may impact their reactivities in various reactions. We report a combined theoretical and experimental study of the initial tautomerization rate of a range of phosphinylidene compounds. Initial tautomerization rates are found to decrease in the order H_3PO_2 > $Ph_2P(O)H$ > $(PhO)_2P(O)H$ > $PhP(O)(OAlk)H$ > $AlkP(O)(OAlk)H$ ≈ $(AlkO)_2P(O)H$, where "Alk" denotes an alkyl substituent. The combination of computational investigations with experimental validation establishes a quantitative measure for the reactivity of various phosphorus compounds, as well as an accurate predictive tool.

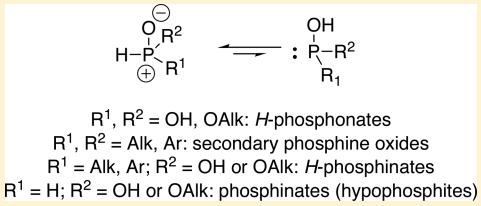

INTRODUCTION

Organophosphorus compounds are critically important in the synthesis of pharmaceuticals, herbicides, pesticides, and phosphine ligands. Methods for formation of phosphorus−carbon bonds continue to receive a great deal of attention.[1] Phosphinylidene[2] (hydrophosphoryl) compounds **1** are an important family of organophosphorus compounds, which includes phosphinates (hypophosphites) **2**, *H*-phosphonates **3**, *H*-phosphinates **4**, and secondary phosphine oxides **5** (Figure 1).

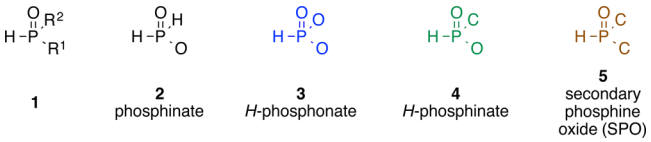

Figure 1. Important types of phosphinylidene compounds.

Tautomerization is an important class of chemical reactions involving the interconversion of constitutional isomers (tautomers). A common subclass is prototropy, in which a hydrogen atom moves from one atom to another. Perhaps the best-known example is the keto−enol tautomerism taught in sophomore organic classes. The phosphinylidene moiety also displays prototropic tautomerism (eq 1).

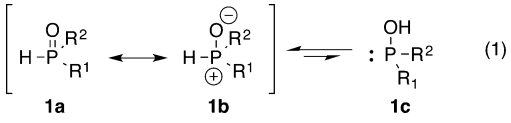

(1)

Phosphinylidenes' prototropic tautomerism appears to be critical to their reactivity.[3] The so-called P(V) form **1a**/**1b** is almost invariably the most stable species.[3a,b] (Note that strong electron acceptors such as R^1 = R^2 = CF_3 can make **1c** more stable,[4] that the issue of the best representation between the classic P(V) form **1a** and the phosphonium form **1b** has been previously studied,[5] and that the resonance form **1b** must be more heavily represented on the basis of electronegativities.) In contrast, the less stable P(III) form **1c** is the reactive species in most reactions involving phosphinylidenes. For example, dimethyl *H*-phosphonate's reaction with chloroacetone is proposed to proceed through base-catalyzed tautomerization.[6] Catalyzed imine hydrophosphonylation is proposed to involve the catalyst's stabilization of the P(III) phosphite.[7] One of us proposed that base-promoted alkylation of alkyl phosphinates and *H*-phosphinates involved base-catalyzed tautomerization or stabilization of deprotonated P(III).[8,9] Several reactions involve trapping the P(III) form by coordination to transition-metal complexes[10] or Lewis acids,[11] or through silylation. Reference 12 reviews additional evidence for the reactivity of **1c**.

Substituent effects on tautomerism are particularly critical for phosphinylidene reactivity. While the equilibrium in eq 1 generally lies far toward the P(V) form, small electronic differences due to substituents R^1 and R^2 dramatically affect the overall rates of reactions involving phosphinylidenes. For example, the "special" reactivity of aryl *H*-phosphinates **4** (R^1 = aryl, R^2 = OAlk) in addition to alkenes has been attributed to stabilization of the P(III) lone pair in **1c** through the aryl's electron-withdrawing effect.[13−15] However, it is at present unclear whether these substituent effects arise from thermodynamic stabilization of the reactive species **1c**, from kinetic acceleration of the rate of **1c** formation, or from other effects. Thus, a fundamental understanding of substituent effects on eq 1 is critical to the practical development of new synthetic organophosphorus chemistry.

Received: July 13, 2015
Published: September 15, 2015

DOI: 10.1021/acs.joc.5b01618
J. Org. Chem. 2015, 80, 10025−10032

Scheme 1. Deuteration of Phosphinylidene Compounds Using an Excess of D_2O

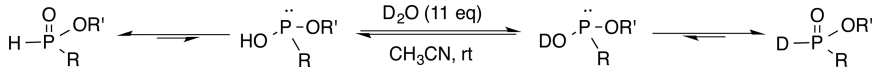

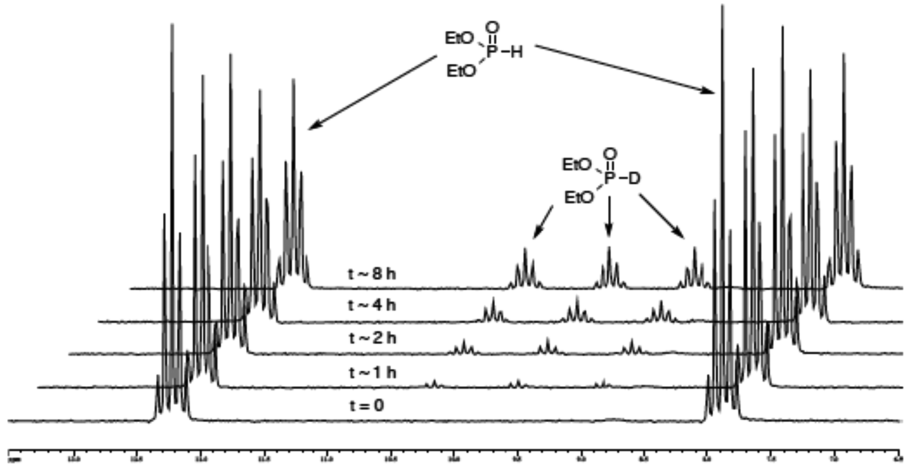

Figure 2. Proton-coupled ^{31}P NMR spectra at 161.97 MHz obtained during the deuteration of diethyl *H*-phosphonate (1 M in CH_3CN) using D_2O (11 equiv) at room temperature: $(EtO)_2P(O)H$, δ 10.05 (dq, J_{P-H} = 704, $^3J_{P-H}$ = 9 Hz); $(EtO)_2P(O)D$, δ 9.73 (tq, J_{P-D} = 107, $^3J_{P-H}$ = 9 Hz).

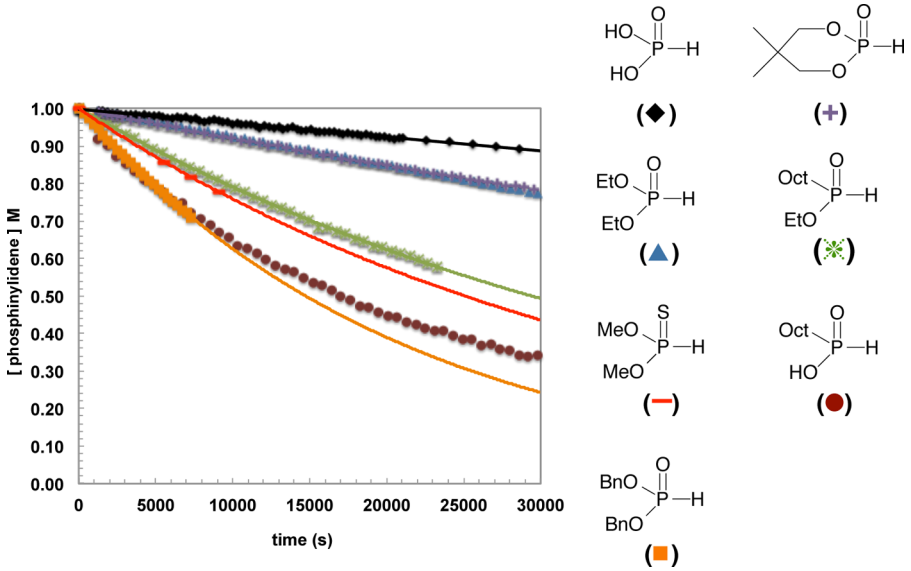

Figure 3. Relative intensity of the P–H starting material's ^{31}P NMR signal (1 M in CH_3CN) during deuteration with D_2O. The figure depicts compounds with half-lives greater than 3 h.

There have been several previous systematic computational studies of how groups R^1 and R^2 affect the thermodynamics of phosphinylidene tautomerization. These largely bear out the trends discussed above, with electron donor groups destabilizing the P(III) form and electron acceptor groups stabilizing the P(III) form.[4,5] Computational studies have also demonstrated that the tautomerization in eq 1 requires catalysis. Uncatalyzed tautomerization of phosphine oxide (R^1 = R^2 = H) proceeds through a strained three-membered ring, and has a prohibitively high predicted reaction barrier of ~60 kcal mol^{-1}.[5,16,17] Substantially lower tautomerization barriers are predicted when P(V) dimers exchange a pair of protons,[18−20] or in phosphine oxide complexes with transition metals or bicyclic guanidines.[21]

There have also been a few previous studies of the kinetics of phosphinylidene tautomerization, for special choices of groups R^1 and R^2. Early experimental studies mainly considered the kinetics of oxidation. With the popularization of computational methods, combined experimental and theoretical works have started to appear.[16,18,19,22] However, these previous works each consider only a single specific case of phosphinylidene **1**, or do not combine theory and experiment, making it difficult to draw general conclusions about reactivity.

The present work seeks to remedy this deficiency in the literature. We report a combined experimental and computational study of the initial rate of tautomerization of 17 different phosphinylidenes $R^1R^2P(O)H$ bearing a range of substituents R^1 and R^2. Our results provide a fundamental understanding of substituent effects on phosphinylidene tautomerization kinetics, a frame of reference to rationalize previous experimental results, and a step toward development of new phosphinylidene chemistry.

DOI: 10.1021/acs.joc.5b01618
J. Org. Chem. 2015, 80, 10025−10032

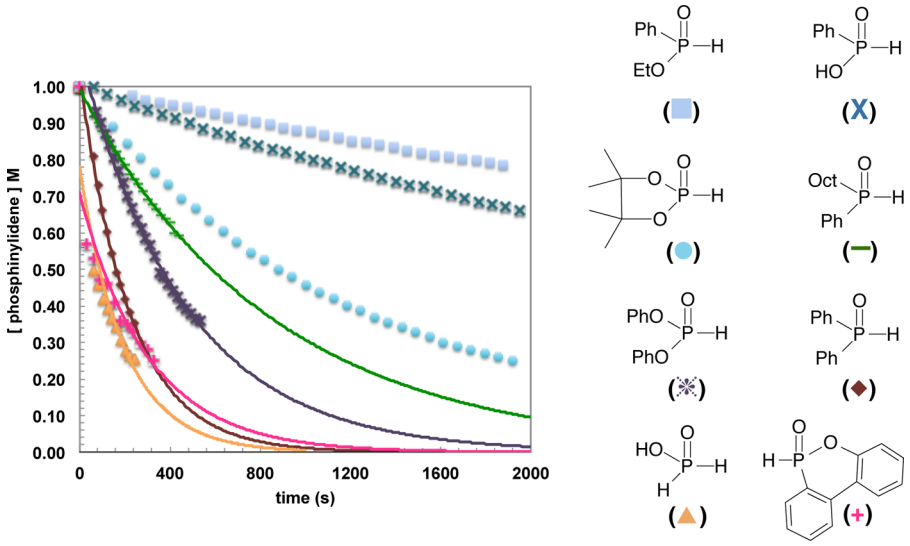

Figure 4. Relative intensity of the P−H starting material's ^{31}P NMR signal (1 M in CH_3CN) during deuteration with D_2O. The figure depicts compounds with half-lives of less than 3 h.

RESULTS AND DISCUSSION

Measured Initial Rates of Deuteration. The kinetics of phosphinylidene tautomerization are directly correlated with the rate of phosphinylidine deuteration by excess D_2O. P(III) phosphinylidines formed by any method will readily exchange the P−OH proton for deuterium, as depicted in Scheme 1. Deuteration rates may be directly observed and quantified over time using ^{31}P NMR spectroscopy as depicted in Figure 2. Excess D_2O ensures that tautomerization is rate-limiting.

Figures 3 and 4 plot the decay of starting material quantified from the ^{31}P NMR spectra. First-order kinetics give excellent fits to the data, with the logarithm of the substrate concentration being nearly linear ($R^2 > 0.99$) with time. Table 1 shows the resulting initial deuteration rates.

Table 1. Pseudo-First-Order Kinetic Data for the Initial Rate of Decay of the Starting Phosphinylidene after Addition of D_2O

entry	R^1	R^2	rate constant (s^{-1})	half-life (s)
1	H	NaO		>3 days
2	Bu	Bu		>3 days
3	OH	OH	3.91×10^{-6}	177366 (49 h)
4	$Me_2C(CH_2O)_2$		8.18×10^{-6}	84695 (24 h)
5	EtO	EtO	9.00×10^{-6}	77025 (21 h)
6	EtO	Oct	2.35×10^{-5}	29446 (8.2 h)
7[a]	$(MeO)_2P(S)H$		2.57×10^{-5}	26992 (7.5 h)
8	OH	Oct	3.55×10^{-5}	19525 (5.4 h)
9	BnO	BnO	4.73×10^{-5}	14648 (4.1 h)
10	EtO	Ph	1.33×10^{-4}	5200 (1.4 h)
11	OH	Ph	2.09×10^{-4}	3324 (55 min)
12	$(Me_2CO)_2$		7.40×10^{-4}	937 (15.6 min)
13	Ph	Oct	1.16×10^{-3}	596 (9.9 min)
14	PhO	PhO	2.20×10^{-3}	315 (5.2 min)
15	Ph	Ph	4.61×10^{-3}	150
16	H	OH	3.87×10^{-3}	179
17	DOPO[b]		2.68×10^{-3}	259

[a]Dimethyl *H*-thiophosphonate. [b]DOPO = 6*H*-Dibenzo[*c*,*e*][1,2λ^5]-oxaphosphinine 6-oxide.

Of the compounds studied, both NaH_2PO_2 (entry 1) and $Bu_2P(O)H$ (entry 2) do not undergo observable deuteration under these conditions, even after several days. This is broadly consistent with the expected effects of these compounds' electron-donating substituents, which should destabilize transition states leading to the reactive P(III) form and stabilize the P(V) form. Other possible effects on $Bu_2P(O)H$ are discussed below. Phosphorous acid (H_3PO_3; entry 3) has the longest observed half-life at around 48 h. Hypophosphorous acid (H_3PO_2; entry 16) reacts 3 orders of magnitude faster than H_3PO_3 with a half-life of only 180 s. This difference in reactivity between H_3PO_2 and H_3PO_3 is consistent with the higher reactivity of H_3PO_2 seen in radical and Pd-catalyzed hydrophosphinylation reactions, and with the lower first pK_a of H_3PO_3 (1.8 versus 2.0, respectively, although the difference is small), meaning that the phosphorus atom is slightly more positively charged in phosphorous acid. In some cases, additional effects might contribute to the dramatic difference between H_3PO_2 and H_3PO_3, including solubility and the pH of the reaction. For example, phosphorous acid is insoluble in organic solvents. and at pH 7 it exists as the dianionic and monoanionic forms (second pK_a = 6.7). In general and for identical "R" groups, phosphinates $ROP(O)H_2$ (**2**) are always more reactive than the corresponding *H*-phosphonates $(RO)_2P(O)H$ (**3**) in all reactions investigated.[23] (Note that it was not possible to measure the rate of deuteration with organic esters of hypophosphorous acid since these compounds are rapidly hydrolyzed to H_3PO_2.)

The observed deuteration rates of phosphinic acid and phosphine oxide derivatives in Table 1 are consistent with the electron donor/acceptor character of substitutents R^1 and R^2. Replacing a −OH group with an *n*-octyl group increases the deuteration rate by a factor of 9 (compare entry 8 to entry 3). Phenyl groups further increase the deuteration rate (entry 11). This confirms the special reactivity of aryl-substituted phosphinylidenes over alkyl-substituted ones, due to their more rapid tautomerization rates. This special reactivity can also be seen in the relative deuteration rates of diphenylphosphine oxide (entry 15), octylphenylphosphine oxide (entry 13), and dibutylphosphine oxide (entry 2).

DOI: 10.1021/acs.joc.5b01618
J. Org. Chem. 2015, 80, 10025−10032

The observed deuteration rates of *H*-phosphonate and *H*-phosphinate esters also showed comparable results with regard to the substituent effect on the rate of deuteration. However, the rates are overall slightly slower than those of the corresponding phosphinic acid and phosphine oxide derivatives. *H*-Phosphonate deuteration rates increased along the series neopentylene glycol *H*-phosphonate < diethyl *H*-phosphonate < dibenzyl *H*-phosphonate < diphenyl *H*-phosphonate (entry 4 < entry 5 < entry 9 < entry 13). This is again consistent with the substitutent effects, and is confirmed experimentally.[9] Replacement of ethoxy with a phenyl group accelerates the reaction (compare entries 5 and 10). Notably, dimethyl thio-*H*-phosphonate (entry 7) shows an increase in the deuteration rate consistent with less stabilization of the positive charge at phosphorus by the sulfur atom.

COMPUTATIONAL RESULTS

Choice of Basis Set. The remainder of this work uses electronic structure calculations to help rationalize the initial deuteration rates in Table 1. We would prefer to use relatively inexpensive Kohn−Sham density functional theory (DFT) calculations in modest atom-centered Gaussian basis sets, an approximation that is enormously successful in many areas.[24,25] However, ref 5 suggests that accurate calculations of the gas-phase tautomerization energy (ΔE) of phosphine oxide ($R^1 = R^2 = H$) require very large basis sets. Before continuing, we thus test whether the widely used[25] B3LYP/6-311++G(3df,3pd) approximation suffices to model phosphine oxide tautomerization.

Table 2 reports the basis set dependence of B3LYP DFT calculations on phosphine oxide's P(V) → P(III) tautomerization energy (ΔE). Positive values mean that P(V) is more stable, a sign convention opposite that of ref 5. P(III) is taken to be in the *trans*-phosphinous acid form (the phosphorus lone pair and the P−OH hydrogen are on the same side of the molecule). B3LYP calculations in the large cc-pV(Q+d)Z basis set give a tautomerization energy within 0.9 kcal mol^{-1} of the reference. The smaller 6-311++G(3df,3pd) basis gives results within 1.6 kcal mol^{-1} of the reference. Both values are well within the ∼4−5 kcal mol^{-1} weighted mean absolute deviation seen for typical DFT calculations on general main group thermochemistry, kinetics, and noncovalent interactions.[24] Smaller basis sets degrade the results, consistent with the importance of phosphorus hypervalency. The B3LYP/6-311++G(3df,3pd) approximation thus appears appropriate for the present work.

Table 2. Number of Basis Functions and Computed P(V) → P(III) Tautomerization Energy (ΔE, kcal mol^{-1}) from B3LYP Calculations on Phosphine Oxide Using Various Basis Sets

basis set	no. of basis functions	ΔE
6-31G(d)	40	−3.29
6-311++G(2d,2p)	96	−2.59
6-311++G(3df,3pd)	155	−0.35
cc-pV(Q+d)Z	255	0.31
ref 5		1.22

Tautomerization Equilibria. We next consider the predicted tautomerization equilibria of the tested phosphinylidene derivatives. Table 3 reports the B3LYP/6-311++G(3df,3pd) tautomerization energy (ΔE) and the P(V) form's computed P−H and P═O bond lengths. As in Table 1, results are sorted from lowest to highest experimental deuteration rates. The results are generally consistent with ref 22. Test calculations on $R^1 = R^2 = H$ (phosphine oxide) and $R^1 = R^2 = CF_3$ (ref 7) are included for comparison. Consistent with previous work,[3] all experimentally tested phosphinylidenes have $\Delta E > 5$ kcal mol^{-1}, suggesting that the P(V) form dominates the equilibrium. $R^1 = R^2 = CF_3$ has the P(III) form more stable, consistent with ref 7. The initial rate of phosphinylidene deuteration will thus be dominated by the rate of the forward reaction P(V) → P(III) in eq 1.

Table 3. B3LYP/6-311++G(3df,3pd) Tautomerization Energy (ΔE, kcal mol^{-1}) and P(V) Form P−H and P═O Bond Lengths (Å) for the Phosphinylidenes in Table 1 and Some Test Cases[a]

entry	R^1	R^2	ΔE	R(P−H)	R(P═O)
1	H	NaO	24.7	1.439	1.499
2	Bu	Bu	7.8	1.417	1.481
3	OH	OH	10.0	1.393	1.465
4	$Me_2C(CH_2O)_2$		6.4	1.393	1.463
5	EtO	EtO	10.2	1.396	1.466
6	EtO	Oct	10.2	1.413	1.472
7	$(MeO)_2P(S)H$		9.8	1.399	1.923
8	OH	Oct	9.8	1.409	1.471
9	BnO	BnO	10.8	1.395	1.468
10	EtO	Ph	9.9	1.404	1.472
11	OH	Ph	9.2	1.404	1.471
12	$(Me_2CO)_2$		7.5	1.397	1.459
13	Ph	Oct	7.2	1.416	1.481
14	PhO	PhO	9.2	1.395	1.462
15	Ph	Ph	6.8	1.415	1.482
16	H	OH	7.0	1.404	1.468
17	DOPO		5.4	1.403	1.467
	H	H	−0.3	1.412	1.477
	CF_3	CF_3	−5.7	1.409	1.465

[a]Positive values indicate that the P(V) form is more stable.

Table 3 shows that tautomerization energies match some, but not all, of the trends in the deuteration initial rates in Table 1. For example, phosphine oxides R^1, R^2 = (OH, OH) < (EtO, EtO) < (BnO, BnO) have increasing deuteration rates but decreasing stability of the P(III) form. Replacing a OH group with an alkyl group gives a substantial increase in deuteration rate but a negligible change in predicted equilibrium (compare entry 8 to entry 3). This is consistent with our hypothesis that deuteration initial rates are dominated by the kinetics, not the thermodynamics, of eq 1. Table 3 also shows that computed P(V)═O bond lengths tend to increase with the deuteration rate, suggesting that more "product-like" P(V) structures with longer P═O bonds give faster tautomerization. *H*-Phosphonates R^1, R^2 = (PhO, PhO), (H, OH), $(Me_2CO)_2$, and DOPO are exceptions.

Choice of Model Solvent. As discussed above, the high barrier computed for gas-phase phosphinylidene tautomerization suggests that this tautomerization must be catalyzed.[16−21] Under our experimental conditions, the catalyst is likely phospinylidene dimerization or the 11 equiv of D_2O. Simulations of deuteration initial rates (i.e., the rate of the forward reaction in eq 1) must account for catalysis by water. Simulations of such solvent effects may either treat the solvent as a continuum or treat explicit solvation by ∼1−10 solvent molecules.[26] Here we explore how implicit and explicit solvent models, and Gibbs free energy corrections, affect the predicted

DOI: 10.1021/acs.joc.5b01618
J. Org. Chem. 2015, 80, 10025−10032

rate of phosphine oxide tautomerization. Table 4 shows the total and Gibbs free energy barriers computed for uncatalyzed tautomerization and for three solvent models: continuum solvent, one explicit H_2O molecule, and two explicit H_2O molecules. Figure 5 shows the computed transition-state geometries. Energies of the initial P(V)−explicit water complexes are included for completeness.

Table 4. B3LYP/6-311++G(3df,3pd) Total Energy Barrier ($\Delta E^{\ddagger}$) and Gibbs Free Energy Barrier ($\Delta G^{\ddagger}$) for Phosphine Oxide P(V) → P(III) Tautomerization[a]

catalyst	$\Delta E^{\ddagger}$	$\Delta G^{\ddagger}$	ΔE_r	ΔG_r
uncatalyzed	62.3	59.1		
continuum water	65.3	62.0		
one explicit H_2O molecule	28.2	36.8	−6.2	0.5
two explicit H_2O molecules	9.3	28.7	−16.2	5.2

[a]Results are reported for uncatalyzed tautomerization and three models of water-catalyzed tautomerization: implicit water, one explicit H_2O molecule, and two explicit H_2O molecules. Energies are relative to isolated P(V) H_3PO and isolated water. Relative energies ΔE_r and ΔG_r of P(V) H_3PO complexed with explicit solvent are included for comparison. All values are given in kilocalories per mole.

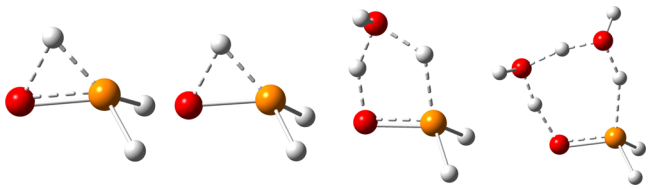

Figure 5. Calculated transition-state geometries for the H_3PO tautomerizations in Table 3. From left to right, the figure shows uncatalyzed tautomerization, tautomerization in continuum water, and tautomerization catalyzed by one and two explicit H_2O molecules.

Table 4 and Figure 5 show that uncatalyzed tautomerization has a strained three-membered ring transition state and a prohibitively high barrier, consistent with previous work.[5] Continuum solvent does not capture water's catalytic effect, giving tautomerization barriers that are even higher than those of the uncatalyzed reaction. Test calculations (Supporting Information) confirm that tested phosphinylidene derivatives have high uncatalyzed and continuum solvent tautomerization barriers. In contrast, a single water molecule dramatically reduces $\Delta E^{\ddagger}$ and $\Delta G^{\ddagger}$ by simultaneously accepting a proton from P and donating a proton to O. Adding a second explicit H_2O gives a less strained transition state and a lower $\Delta E^{\ddagger}$. However, the entropic cost of ordering the second water molecule yields only a modest effect on $\Delta G^{\ddagger}$. These results suggest that one explicit H_2O provides a qualitatively correct treatment of water-catalyzed tautomerization, making it a reasonable model system for exploring substituent effects on deuteration initial rates.

Tautomerization Mechanism. Figure 5 illustrates that water-catalyzed phosphinylidene tautomerization involves simultaneous dissociation of a P−H bond and formation of an O−H bond. Figure 6 reports intrinsic reaction coordinate (IRC) calculations[27] of the P(V) → P(III) tautomerization reaction coordinate. Reaction coordinates are visualized as functions of two variables, the lengths of the forming O−H and breaking P−H bonds. Uncatalyzed and catalyzed P(V) → P(III) tautomerizations begin with contraction of the complex. The O−H bond shrinks by ∼0.4 Å, and the dissociating P−H bond undergoes a small contraction in the water-catalyzed tautomerization. The complex then undergoes simultaneous O−H bond shortening and P−H bond lengthening, passing through the transition states shown in Figure 5. Barrier heights are inversely correlated with the transition state's P−H bond length. Once the O−H bond approaches its equilibrium value, the complex re-expands, lengthening the P−H bond to form the P(III) product. As in Table 3, these results suggest that product-like species with a soft and readily dissociated P−H bond will tend to have lower reaction barriers.

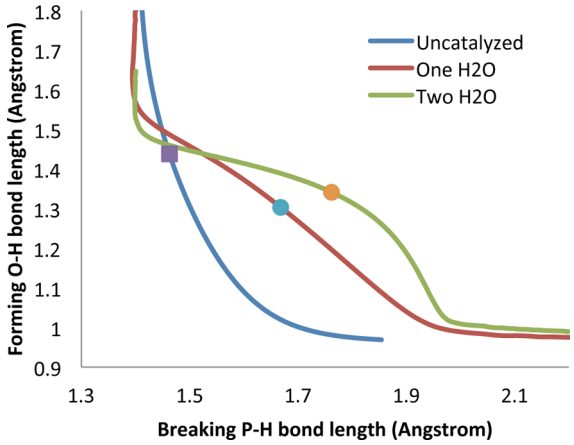

Figure 6. Computed reaction paths for the H_3PO tautomerizations in Table 3, plotted as functions of the P−H and O−H bond lengths. Points denote the positions of the transition states.

Predicted Deuteration Initial Rates. We next compare the experimental deuteration initial rates in Table 1 to simulations. As discussed in the Computational Methods, deuteration half-lives are predicted from rate constants given by the Eyring equation, using the B3LYP/6-311++G(3df,3pd) total energy barrier ($\Delta E^{\ddagger}$) to P(V) tautomerization catalyzed by a single H_2O molecule. Table 5 reports the computed total energy barriers. Figure 7 presents the correlation between computed and experimental deuteration half-lives.

Figure 6 shows that the computed H_2O-catalyzed half-lives recover most experimental trends. Computed *H*-phosphinate half-lives follow experimental trends: (EtO, Oct) > (OH, Oct) > (EtO, Ph) > (OH, Ph) > (OH, H) > DOPO (entry 6 > entry 8 > entry 10 > entry 11 > entry 16 > entry 17). Conputed *H*-phosphonate half-lives also follow experimental trends: (EtO, EtO) ≈ $(CH_3)_2C(CH_2O)_2$ > $(MeO)_2P(S)H$ > (PhO, PhO) (entries 5 and 4 > entry 7 > entry 14). Computed half-lives capture the special reactivity of aryl phosphinylidenes: (EtO, Ph), (OH, Ph), and (Ph, Oct) have lower tautomerization barriers than (EtO, Oct), (OH, Oct), and (Bu, Bu), respectively (entries 10 and 6, 11 and 8, 13 and 2). Computed half-lives also capture trends among different classes of phosphinylidenes. Secondary phosphine oxides (SPOs) have short half-lives, while *H*-phosphonates tend to have rather long half-lives. The calculations are not a perfect representation of experiment: computed tautomerization barriers are ∼10 kcal/mol too high, giving half-lives that are ∼8 orders of magnitude too large. However, the good agreement of trends supports our previous arguments that this model suffices to capture this system's chemistry.

DOI: 10.1021/acs.joc.5b01618
J. Org. Chem. 2015, 80, 10025−10032

Table 5. B3LYP/6-311++G(3df,3pd) Tautomerization Energy Barrier ($\Delta E^{\ddagger}$, kcal mol^{-1}) and Transition-State P−H and P═O Bond Lengths (Å) for the Phosphinylidenes in Table 1 and Some Test Cases[a]

entry	R^1	R^2	$\Delta E^{\ddagger}$	R(P−H)	R(P═O)
1	H	NaO			
2	Bu	Bu	31.3	1.596	1.572
3	OH	OH			
4	$Me_2C(CH_2O)_2$		35.4	1.725	1.529
5	EtO	EtO	36.8	1.712	1.537
6	EtO	Oct	35.1	1.646	1.559
7	$(MeO)_2P(S)H$		33.5	1.842	2.046
8	OH	Oct	34.9	1.668	1.554
9	BnO	BnO			
10	EtO	Ph	33.5	1.640	1.560
11	OH	Ph	33.4	1.676	1.553
12	$(Me_2CO)_2$		33.1	1.717	1.537
13	Ph	Oct	30.8	1.615	1.570
14	PhO	PhO	34.4	1.749	1.538
15	Ph	Ph	30.8	1.625	1.569
16	H	OH	32.7	1.695	1.547
17	DOPO		31.6	1.682	1.548
	H	H	28.2	1.668	1.557
	CF_3	CF_3	24.2	1.745	1.527

[a]The calculations treat catalysis by a single H_2O molecule.

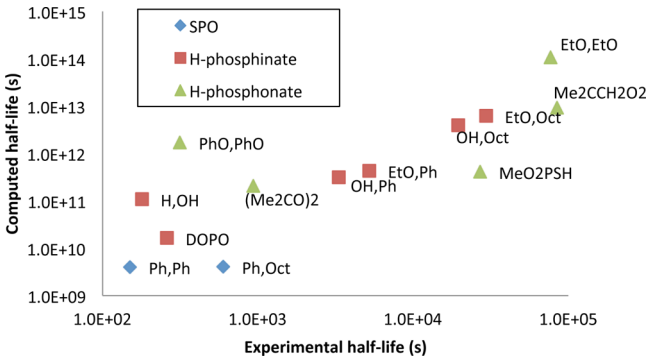

Figure 7. Calculated vs experimental deuteration half-lives.

Table 5 also provides chemical insight into substituent effects on tautomerization and deuteration. There is a modest correlation between the measured deuteration rate and the computed transition-state P−H bond length, with fast deuteration generally corresponding to long bond lengths. This is consistent with the above results suggesting that soft, product-like P−H bonds yield faster tautomerization. In contrast, transition-state P═O bond lengths are not well correlated with experiment, suggesting that the tautomerization rate is more affected by the P−H bond.

One notable result in Tables 3 and 5 is that the secondary phosphine oxide $R^1 = R^2$ = Bu (entry 1) has a long P(V)═O bond and a low predicted $\Delta E^{\ddagger}$. These results are consistent with the computed and experimental results for other secondary phosphine oxides (entries 13 and 15), but are inconsistent with the negligible deuteration rate measured for entry 1. We speculate that other effects, such as aggregation, may play a role in the slow deuteration of this species. Steric effects may also play a role since the angle between the two substituents decreases from P(V) to P(III).

CONCLUSIONS

The experimental and computational results reported here show that many of the known trends in phosphinylidene $R^1R^2P(O)H$ reactivity, such as metal-catalyzed and free radical addition to hydrocarbons, are correlated with the rate of prototropic tautomerism. Measured deuteration initial rates yield a quantitative measure of relative reactivities. The ease of tautomerization is found to be H_3PO_2 > $Ph_2P(O)H$ > $(PhO)_2P(O)H$ > PhP(O)(OAlk)H > AlkP(O)(OAlk)H ≈ $(AlkO)_2P(O)H$. Deuteration half-lives computed from H_2O-catalyzed tautomerization barriers capture most experimental trends, indicating the promise of computation for predictive studies of phosphinylidene reactivity. Calculations also suggest that substituents yielding soft, product-like P(V)−H bonds will tend to increase tautomerization rates. Phosphorus chemists should pay attention to the large differences in tautomerization rates and the associated chemical reactivity between the various phosphinylidene compounds when interpreting and evaluating the scope of a particular methodology.

EXPERIMENTAL SECTION

General Chemistry. All starting materials were purchased from commercial sources and used as received. The solvents were distilled under N_2 and dried according to standard procedures (toluene and acetonitrile from CaH_2, THF from Na/benzophenone ketyl; *N,N*-diisopropylethylamine was distilled from CaH_2 and stored over 4 Å molecular sieves). TLC analyses were performed on sheets precoated with silica gel $60F_{254}$. Compound detection was achieved by exposure to UV light (254 nm) and by immersion in anisaldehyde stain (by volume, 93% ethanol, 3.5% H_2SO_4, 1% AcOH, and 2.5% anisaldehyde) followed by heating at 150 °C. Flash chromatography experiments were carried out on silica gel (premium Rf grade) (40−75 μm). Ethyl acetate/hexane mixtures were used as the eluent for chromatographic purifications. The ^{1}H, ^{13}C, and ^{31}P NMR spectra were recorded on a 400 MHz spectrometer. Chemical shifts for ^{1}H NMR are given in parts per million relative to internal tetramethylsilane (δ = 0 ppm), using $CDCl_3$ as the solvent. Chemical shifts for ^{13}C NMR are given in parts per million relative to $CDCl_3$ (δ = 77.0 ppm). Chemical shifts for ^{31}P NMR spectra are recorded at 161.97 MHz and given relative to external 85% phosphoric acid (δ = 0 ppm). Abbreviations used for signal patterns are as follows: s, singlet; d, doublet; t, triplet; q, quadruplet; m, multiplet.

Procedure for the Collection of Kinetic Data via ^{31}P NMR for Structure Influence Studies. NMR kinetics were recorded at room temperature on a 400 MHz spectrometer, at 161.97 MHz for ^{31}P using D_2O as a solvent lock, with four repetitions, a 2 s relaxation delay, and a 45° pulse angle. Delays between each scan were dependent on the substrate run (see the Supporting Information for more details). The NMR spectra were individually processed and integrated using appropriate software. Each resonance for the P−H compound and the forming P−D compounds was individually integrated, and the total sum of integrals was normalized to 100%. The kinetics were calculated on the basis of the decay of starting P−H compound (i.e., total integrals for starting material (SM)/100 × concentration of sample, 1 M). The NMR yields are determined by integration of all the resonances in the ^{31}P spectra.

Phosphinylidene compounds were diluted to 1 M using freshly distilled CH_3CN in a 4 dram glass vial (note that solutions should be stored in the freezer when not in use). By 1 mL syringe, 0.5 mL of phosphinylidene solution (0.5 mmol) was added to a dry NMR tube, and the tube was capped until the solution was needed. D_2O (99.99 atom %, no internal reference, 0.1 mL, 5.5 mmol, 11 equiv) was added by autopipet, the tube was recapped, and the tube was inverted one time to mix the solution. The time from the addition of D_2O to the start of the data collection was noted. Spectra were collected over regular time intervals at room temperature using four transients as predetermined by running a test sample, which was also used as a

DOI: 10.1021/acs.joc.5b01618
J. Org. Chem. 2015, 80, 10025−10032

reference sample to lock, tune, and shim the spectrometer before each run. The NMR kinetic experiments were completed in duplicate for each phosphinylidene sample.

Preparation of Phosphinylidene Compounds. Diethyl phosphite, diphenyl phosphite, dibenzyl phosphite, phenylphosphinic acid, DOPO, and sodium hypophosphite were all used as purchased without further purification. Hypophosphorous and phosphorus acids were acquired as 50 wt % solutions in water and preconcentrated in vacuo at rt for 15 min before use. All other phosphinylidene compounds used for the kinetic studies were synthesized according to literature procedures.

Dibutylphosphine Oxide (Table 1, Entry 2). This compound was prepared from diethyl phosphite according to a literature procedure.[28] Yield: 3.44 g (70%). ^{1}H NMR (400 MHz, $CDCl_3$): δ 6.81 (d, J_{P-H} = 446 Hz, 1H), 1.81 (m, 4H), 1.63 (m, 4H), 0.968 (t, J = 7.4 Hz, 6H). ^{31}P NMR (162 MHz, $CDCl_3$): δ 34.9 (dm, J_{P-H} = 455 Hz).

5,5-Dimethyl-1,3,2-dioxaphosphinane 2-Oxide (Table 1, Entry 5). Aqueous H_3PO_3 (50 wt %, 8.2 g, 50 mmol) was weighed into a 250 mL round-bottom flask along with 2,2-dimethyl-1,3-propanediol (5.21 g, 50 mmol). Toluene (100 mL) was added, and a Dean−Stark trap prefilled with excess toluene was fitted onto the flask. The solution was refluxed overnight (~16 h) under N_2. After cooling, column chromatography on silica gel (80:20 hexanes/EtOAc to 100% EtOAc) was completed to obtain a white solid (3.53 g, 47%). ^{1}H NMR (400 MHz, $CDCl_3$): δ 6.92 (d, J_{P-H} = 676 Hz, 1H), 4.06 (m, 4H), 1.26 (s, 3H), 0.942 (s, 3H). ^{31}P NMR (162 MHz, $CDCl_3$): δ 3.02 (dm, J_{P-H} = 671 Hz). Spectral properties match previously reported values.[29]

Ethyl Octylphosphinate (Table 1, Entry 6). This compound was prepared from octylphosphinic acid according to a literature procedure.[30] After column chromatography on silica gel (80:20 hexanes/EtOAc to 100% EtOAC), a clear oil was obtained (2.76 g, 67%). ^{1}H NMR (400 MHz, $CDCl_3$): δ 7.09 (d, J_{P-H} = 526 Hz, 1H), 4.17 (m, 2H), 1.74 (m, 2H), 1.58 (m, 2H), 1.42−1.28 (m, 13H), 0.88 (t, J = 6.96 Hz, 3H). ^{31}P NMR (162 MHz, $CDCl_3$): δ 39.1 (dm, J_{P-H} = 526 Hz).

Dimethyl Thiophosphonate (Table 1, Entry 7). This compound was prepared according to a literature procedure.[31] Yield: 1.90 g (30%). ^{1}H NMR (400 MHz, $CDCl_3$): δ 7.36 (d, J_{P-H} = 600 Hz), 3.86 (m, 6H, J = 15 Hz). ^{31}P NMR (162 MHz, $CDCl_3$): δ 75.2 (dm, J_{P-H} = 590 Hz).

Octylphosphinic Acid (Table 1, Entry 8). This compound was prepared according to a literature procedure.[32] Yield: 15.6 g (70%). ^{1}H NMR (400 MHz, $CDCl_3$): δ 12.4 (br, 1H), 7.11 (d, J_{P-H} = 541 Hz), 1.77 (m, 2H), 1.61 (m, 2H), 1.41 (m, 2H), 1.29 (m, 8H), 0.92 (t, J = 7.09 Hz). ^{31}P NMR (162 MHz, $CDCl_3$): δ 34.8 (d, J_{P-H} = 536 Hz).

Ethyl Phenylphosphinate (Table 1, Entry 10). This compound was prepared from phenylphosphinic acid according to a literature procedure.[27] Yield: 2.72 g (80%). ^{1}H NMR (400 MHz, $CDCl_3$): δ 7.61 (d, J_{P-H} = 563 Hz, 1H), 7.80 (m, 2H), 7.62 (m, 1H), 7.55 (m, 2H), 4.18 (m, 2H), 1.40 (t, J = 6.80 Hz, 3H). ^{31}P NMR (162 MHz, $CDCl_3$): δ 24.6 (d, J_{P-H} = 563 Hz).

4,4,5,5-Tetramethyl-1,3,2-dioxaphospholane 2-Oxide (Table 1 Entry 12). This compound was prepared from diethyl phosphite according to a literature procedure.[29] Yield: 2.93 g (17%). ^{1}H NMR (400 MHz, $CDCl_3$): δ 7.22 (d, J_{P-H} = 708 Hz, 1H), 1.48 (s, 6H), 1.38 (s, 6H). ^{31}P NMR (162 MHz, $CDCl_3$): δ 16.7 (d, J_{P-H} = 708 Hz).

Octylphenylphosphine Oxide (Table 1, Entry 13). This compound was prepared according to a literature procedure.[33] Yield: 1.43 g (30%). ^{1}H NMR (400 MHz, $CDCl_3$): δ 7.72 (m, 2H), 7.54 (m, 3H), 7.50 (d, J_{P-H} = 463 Hz, 1H), 2.01 (m, 2H), 1.61 (m, 2H), 1.42 (m, 2H), 1.26 (t, J = 7.08 Hz, 3H). ^{13}C NMR (101 MHz, $CDCl_3$): δ 132.4, 131.2 (d, J_{PC} = 95.6 Hz), 129.9 (d, J_{PCC} = 11.1 Hz), 128.9 (d, J_{PCC} = 13.1 Hz), 31.7. 30.7, 30.6 (d, J = 20.1 Hz), 29.5 (d, J_{PC} = 99.6 Hz), 29.0, 22.6, 21.5 (d, J_{PCCC} = 4.02 Hz), 14.1. ^{31}P NMR (162 MHz, $CDCl_3$): δ 21.4 (d, J_{P-H} = 481 Hz).

Diphenylphosphine Oxide (Table 1, Entry 15). This compound was prepared from chlorodiphenylphosphine according to a literature procedure.[34] Yield: 4.49 g (89%). ^{1}H NMR (400 MHz, $CDCl_3$): δ 8.09 (d, J_{P-H} = 480 Hz, 1H), 7.73 (m, 4H), 7.58 (m, 2H), 7.51 (m, 4H). ^{31}P NMR (162 MHz, $CDCl_3$): δ 21.4 (d, J_{P-H} = 481 Hz).

Computational Methods. Calculations use the Gaussian 09 electronic structure program,[35] generalized Kohn−Sham density functional theory[36,37] with the B3LYP hybrid exchange-correlation functional,[38,39] and Pople-type[40] or cc-pV(Q+d)Z[41−43] basis sets taken from the EMSL Basis Set Exchange.[44] cc-pV(Q+d)Z calculations use the cc-pVQZ basis on hydrogen. Continuum solvent calculations use the SMD model.[45] Alkyl chains are replaced with methyl groups for computational convenience. No constraints on molecular symmetry are applied. All geometries are fully optimized. Local minima and transition states are confirmed to have zero and one negative eigenvalue in their vibrational Hessian. Test calculations on most transition states confirm that displacing the molecule along the Hessian eigenvector with a negative eigenvalue, and reoptimizing the geometry, converges to the expected reactant or product geometry. Additional test calculations using the intrinsic reaction coordinate method confirm that the transition states connect the reactants and products of interest. Entropic and thermal corrections are evaluated for isolated molecules using standard rigid rotor harmonic oscillator approximations. (Put another way, the Gibbs free energy is taken as the "sum of electronic and thermal free energies" printed in a Gaussian 09 vibrational frequency calculation.) Pictures of calculated geometries use color coding: H (white), C (gray), O (red), P (yellow). Bond orders in these pictures are drawn as a guide to the eye. H_2O-catalyzed tautomerization barriers are evaluated as the difference between the transition-state energy and the energy of free H_2O and free P(V) phosphinylidene. The computed deuteration half-lives ($t_{1/2}$ = ln(2)/k) in Figure 6 are calculated from rate constants k obtained using the Eyring equation $k = k_B T/h \exp(-\Delta G^{\ddagger}/RT)$, with T = 298.15 K, and with $\Delta G^{\ddagger}$ approximated as $\Delta E^{\ddagger}$ obtained from B3LYP/6-311++G(3df,3pd) calcuations on the P(V) → P(III) tautomerization barrier, catalyzed by a single explicit H_2O molecule as described above. Computing the barrier relative to the most stable H_2O−P(V) complex gives unrealistic results where R^1 or R^2 is a OH group, as forming the transition state requires breaking hydrogen bonds between P(V) OH groups and the external water. This issue is extreme for H_2O-catalyzed H_3PO_3 and NaH_2PO_2 tautomerization (entries 1 and 3). We were unable to locate transition states for these reactions, as all geometry optimizations converged to give H_2O hydrogen bound to P−OH groups.

■ ASSOCIATED CONTENT

Supporting Information

The Supporting Information is available free of charge on the ACS Publications website at DOI: 10.1021/acs.joc.5b01618.

All computed molecular geometries and energies (TXT)
Kinetic data and graphs and NMR spectra for the compounds in Table 1 (PDF)

■ AUTHOR INFORMATION

Corresponding Authors

*E-mail: b.janesko@tcu.edu.
*E-mail: j.montchamp@tcu.edu.

Notes

The authors declare no competing financial interest.

■ ACKNOWLEDGMENTS

This material is based in part upon work supported by the National Science Foundation under Grant CHE-1262254. Support from the Texas Christian University Invests in Scholarship (TCU-IS) Program is acknowledged for M.A.B. and H.C.F.

■ REFERENCES

(1) (a) Hartley, F. R. *The Chemistry of Organophosphorus Compounds*; Wiley: New York, 1996; Vol. 4. (b) Quin, L. D. *A Guide to Organophosphorus Chemistry*; Wiley: New York, 2000. (c) Flett, D. S. *J. Organomet. Chem.* **2005**, *690*, 2426−2438. (d) Savignac, P., Iorga, B.

DOI: 10.1021/acs.joc.5b01618
J. Org. Chem. 2015, 80, 10025−10032

Modern Phosphonate Chemistry; CRC: Boca Raton, FL, 2003. (e) Corbridge, D. E. C. *Phosphorus: An Outline of Its Chemistry, Biochemistry and Uses*, 5th ed.; Elsevier: Amsterdam, 1995. (f) Büchel, K. H.; Moretto, H.-H.; Woditsch, P. *Industrial Inorganic Chemistry*, 2nd ed.; Wiley-VCH: New York, 2000; pp 65−101. (g) *Kirk-Othmer Encyclopedia of Chemical Technology*, 4th ed.; Wiley: New York, 1999; Vol. *18*.

(2) (a) Nifant'ev, E. E. *Russ. Chem. Rev.* **1978**, *47*, 835−858. (b) Fletcher, J. H.; Dermer, O. C.; Fox, R. B. *Adv. Chem. Ser.* **1974**, *126*, 278−288.

(3) See for example: (a) Guthrie, J. P. *Can. J. Chem.* **1979**, *57*, 236−239. (b) Hammond, P. R. *J. Chem. Soc.* **1962**, 1365. (c) Mehrotra, R. N. *Eur. Chem. Bull.* **2013**, *2*, 758−776. (d) Christiansen, A.; Selent, D.; Spannenberg, A.; Köckerling, M.; Reinke, H.; Baumann, W.; Jiao, H.; Franke, R.; Börner, A. *Chem. - Eur. J.* **2011**, *17*, 2120−2129. (e) Algarra, A. G.; Fernández-Trujillo, M. J.; Hernández-Molina, R.; Basallote, M. G. *Dalton Trans.* **2011**, *40*, 8589−8597. (f) Jung, L.-Y.; Tsai, S.-H.; Hong, F.-E. *Organometallics* **2009**, *28*, 6044−6053. (g) Akbayeva, D. N.; Di Vaira, M.; Constantini, S. S.; Peruzzini, M.; Stoppioni, P. *Dalton Trans.* **2006**, 389−395. (h) Sokolov, M. N.; Chubarova, E. V.; Kovalenko, K. A.; Mironov, I. V.; Virovets, A. V.; Peresypkina, E. V.; Fedin, V. P. *Russ. Chem. Bull.* **2005**, *54*, 615−622. (i) Sharma, P. K. *Indian J. Chem.* **2002**, *41A*, 1612−1615. (j) Chandra, S. K.; Gelerinter, E.; Gould, E. S. *Inorg. Chem.* **1995**, *34*, 4057−4061. (k) Seth, M.; Mathur, A.; Banerji, K. K. *Bull. Chem. Soc. Jpn.* **1990**, *63*, 3640−3643. (l) Sernaglia, R. L.; Franco, D. W. *Inorg. Chem.* **1989**, *28*, 3485−3489. (m) Gallagher, M. J.; Honegger, H. *Tetrahedron Lett.* **1977**, *18*, 2987−2990. (n) Bailey, W. J.; Fox, R. B. *J. Org. Chem.* **1964**, *29*, 1013−1017. (o) Bailey, W. J.; Fox, R. B. *J. Org. Chem.* **1963**, *28*, 531−534. (p) Cherbuliez, E.; Weber, G.; Rabinowitz, J. *Helv. Chim. Acta* **1963**, *46*, 2464−2470.

(4) (a) Griffiths, J. E.; Burg, A. B. *J. Am. Chem. Soc.* **1960**, *82*, 1507−1508. (b) Hoge, B.; Neufeind, S.; Hettel, S.; Wiebe, W.; Thösen, C. *J. Organomet. Chem.* **2005**, *690*, 2382−2387. (c) Kurscheid, B.; Wiebe, W.; Neumann, B.; Stammler, H.-G.; Hoge, B. *Eur. J. Inorg. Chem.* **2011**, *2011*, 5523−5529.

(5) Wesolowski, S. S.; Brinkmann, N. R.; Valeev, E. F.; Schaefer, H. F.; Repasky, M. P.; Jorgensen, W. L. *J. Chem. Phys.* **2002**, *116*, 112.

(6) Springs, B.; Haake, P. *J. Org. Chem.* **1977**, *42*, 472−474.

(7) (a) Akiyama, T.; Morita, H.; Itoh, J.; Fuchibe, K. *Org. Lett.* **2005**, *7*, 2583−2585. (b) Pettersen, D.; Marcolini, M.; Bernardi, L.; Fini, F.; Herrera, R. P.; Sgarzani, V.; Ricci, A. *J. Org. Chem.* **2006**, *71*, 6269−6272.

(8) Abrunhosa-Thomas, I.; Ribière, P.; Adcock, A. C.; Montchamp, J.-L. *Synthesis* **2006**, 325−331.

(9) Gavara, L.; Petit, C.; Montchamp, J.-L. *Tetrahedron Lett.* **2012**, *53*, 5000−5003.

(10) (a) Kraihanzel, C. S.; Bartish, C. M. *J. Am. Chem. Soc.* **1972**, *94*, 3572−3575. (b) Yakhvarov, D.; Caporali, M.; Gonsalvi, L.; Latypov, S.; Mirabello, V.; Rizvanov, I.; Sinyashin, O.; Stoppioni, P.; Peruzzini, M. *Angew. Chem., Int. Ed.* **2011**, *50*, 5370−5373. (c) Manca, G.; Caporali, M.; Ienco, A.; Peruzzini, M.; Mealli, C. *J. Organomet. Chem.* **2014**, *760*, 177−185.

(11) Belabassi, Y.; Antczak, M. I.; Tellez, J.; Montchamp, J.-L. *Tetrahedron* **2008**, *64*, 9181−9190.

(12) (a) Montchamp, J.-L. *Acc. Chem. Res.* **2014**, *47*, 77−87. (b) Montchamp, J.-L. *Phosphorus, Sulfur Silicon Relat. Elem.* **2013**, *188*, 66−75.

(13) Han, L.-B.; Zhao, C.-Q.; Onozawa, S.; Goto, M.; Tanaka, M. *J. Am. Chem. Soc.* **2002**, *124*, 3842−3843.

(14) Han, L.-B.; Zhang, C.; Yazawa, H.; Shimada, S. *J. Am. Chem. Soc.* **2004**, *126*, 5080−5081.

(15) Petit, C.; Fécourt, F.; Montchamp, J.-L. *Adv. Synth. Catal.* **2011**, *353*, 1883−1888.

(16) Chesnut, D. B. *Heteroat. Chem.* **2000**, *11*, 73−80.

(17) Boatz, J. A.; Schmidt, M. W.; Gordon, M. S. *J. Phys. Chem.* **1987**, *91*, 1743−1749.

(18) Babin, Y. V.; Prisyazhnyuk, A. V.; Ustynyuk, Y. A. *Russ. J. Phys. Chem. A* **2008**, *82*, 94−100.

(19) Prisyazhnyuk, A. V.; Babin, Y. V. *J. Struct. Chem.* **2005**, *46*, 164−167.

(20) Mamaev, V. M.; Prisyajnuk, A. V.; Laikov, D. N.; Logutenko, L. S.; Babin, Y. V. *Mendeleev Commun.* **1999**, *9*, 240−241.

(21) Cho, B.; Tan, C.-H.; Wong, M. W. *Org. Biomol. Chem.* **2011**, *9*, 4550−4557.

(22) (a) Babin, Y. V.; Ustynyuk, Y. A. *Russ. J. Phys. Chem. A* **2007**, *81*, 1810−1819. (b) Ustynyuk, Yu. A.; Babin, Yu. V. *Russ. J. Gen. Chem.* **2008**, *78*, 822−832.

(23) See for example: (a) Deprèle, S.; Montchamp, J.-L. *J. Org. Chem.* **2001**, *66*, 6745−6755. (b) Deprèle, S.; Montchamp, J.-L. *J. Organomet. Chem.* **2002**, *643*−*644*, 154−163. (c) Deprèle, S.; Montchamp, J.-L. *J. Am. Chem. Soc.* **2002**, *124*, 9386−9387. (d) Deprèle, S.; Montchamp, J.-L. *Org. Lett.* **2004**, *6*, 3805−3808. (e) Ribière, P.; Bravo-Altamirano, K.; Antczak, M. I.; Hawkins, J. D.; Montchamp, J.-L. *J. Org. Chem.* **2005**, *70*, 4064−4072. (f) Fisher, H. C.; Prost, L.; Montchamp, J.-L. *Eur. J. Org. Chem.* **2013**, *2013*, 7973−7978.

(24) Goerigk, L.; Grimme, S. *Phys. Chem. Chem. Phys.* **2011**, *13*, 6670−6688.

(25) Becke, A. D. *J. Chem. Phys.* **2014**, *140*, 18A301−18A301.

(26) Cramer, C. J.; Truhlar, D. G. *Acc. Chem. Res.* **2008**, *41*, 760−768.

(27) Hratchian, H. P.; Schlegel, H. B. *J. Chem. Phys.* **2004**, *120*, 9918−9924.

(28) Busacca, C. A.; Lorenz, J. C.; Grinberg, N.; Haddad, N.; Hrapchak, M.; Latli, B.; Lee, H.; Sabila, P.; Saha, A.; Sarvestani, M.; Shen, S.; Varsolona, R.; Wei, X.; Senanayake, C. H. *Org. Lett.* **2005**, *7*, 4277−4280.

(29) Maffei, M.; Buono, G. *Tetrahedron* **2003**, *59*, 8821−8825.

(30) Dumond, Y.; Baker, R.; Montchamp, J. *Org. Lett.* **2000**, *2*, 3341−3344.

(31) McKenna, C. E. (The University of Southern California). Improved Preparations of Thiophosphites and Thiophosphonates. US Patent 6,284,909, Sept 4, 2001.

(32) Ortial, S.; Fisher, H. C.; Montchamp, J.-L. *J. Org. Chem.* **2013**, *78*, 6599−6608.

(33) Gatrone, R. C.; Kaplan, L.; Philip Horwitz, E. *Solvent Extr. Ion Exch.* **1987**, *5*, 1075−1116.

(34) Shioji, K.; Matsumoto, A.; Takao, M.; Kurauchi, Y.; Shigetomi, T.; Yokomori, Y.; Okuma, K. *Bull. Chem. Soc. Jpn.* **2007**, *80*, 743−746.

(35) Frisch, M. J.; Trucks, G. W.; Schlegel, H. B.; Scuseria, G. E.; Robb, M. A.; Cheeseman, J. R.; Scalmani, G.; Barone, V.; Mennucci, B.; Petersson, G. A.; Nakatsuji, H.; Caricato, M.; Li, X.; Hratchian, H. P.; Izmaylov, A. F.; Bloino, J.; Zheng, G.; Sonnenberg, J. L.; Hada, M.; Ehara, M.; Toyota, K.; Fukuda, R.; Hasegawa, J.; Ishida, M.; Nakajima, T.; Honda, Y.; Kitao, O.; Nakai, H.; Vreven, T.; Montgomery, J. A., Jr.; Peralta, J. E.; Ogliaro, F.; Bearpark, M.; Heyd, J. J.; Brothers, E.; Kudin, K. N.; Staroverov, V. N.; Kobayashi, R.; Normand, J.; Raghavachari, K.; Rendell, A.; Burant, J. C.; Iyengar, S. S.; Tomasi, J.; Cossi, M.; Rega, N.; Millam, J. M.; Klene, M.; Knox, J. E.; Cross, J. B.; Bakken, V.; Adamo, C.; Jaramillo, J.; Gomperts, R.; Stratmann, R. E.; Yazyev, O.; Austin, A. J.; Cammi, R.; Pomelli, C.; Ochterski, J. W.; Martin, R. L.; Morokuma, K.; Zakrzewski, V. G.; Voth, G. A.; Salvador, P.; Dannenberg, J. J.; Dapprich, S.; Daniels, A. D.; Ö. Farkas, Foresman, J. B.; Ortiz, J. V.; Cioslowski, J.; Fox, D. J. *Gaussian 09*, revision D.01; Gaussian, Inc.: Wallingford, CT, 2009.

(36) Hohenberg, P.; Kohn, W. *Phys. Rev.* **1964**, *136*, B864.

(37) Kohn, W.; Sham, L. J. *Phys. Rev.* **1965**, *140*, A1133.

(38) Becke, A. D. *J. Chem. Phys.* **1993**, *98*, 5648.

(39) Stephens, P.; Devlin, F.; Chabalowski, C. F.; Frisch, M. J. *J. Phys. Chem.* **1994**, *98*, 11623−11627.

(40) Hehre, W. J.; Ditchfield, R.; Pople, J. A. *J. Chem. Phys.* **1972**, *56*, 2257−2261.

(41) Dunning, T. H. *J. Chem. Phys.* **1989**, *90*, 1007.

(42) Dunning, T. H. *J. Phys. Chem. A* **2000**, *104*, 9062−9080.

(43) Dunning, T. H.; Peterson, K. A.; Wilson, A. K. *J. Chem. Phys.* **2001**, *114*, 9244−9253.

(44) Feller, D. *J. Comput. Chem.* **1996**, *17*, 1571−1586.

(45) Marenich, A. V.; Cramer, C. J.; Truhlar, D. G. *J. Phys. Chem. B* **2009**, *113*, 6378−6396.

DOI: 10.1021/acs.joc.5b01618
J. Org. Chem. 2015, 80, 10025−10032